Hydrogentrimethylammonium: A Marginally Stable Hypervalent Radical

Scott A. Shaffer and František Tureček*

Contribution from the Department of Chemistry, BG-10, University of Washington, Seattle, Washington 98195

Received August 2, 1993. Revised Manuscript Received July 12, 1994[⊕]

Abstract: Hydrogentrimethylammonium, $(CH_3)_3NH^•$, **1**, and its deuterium-labeled isotopomers are generated by collisional neutralization with dimethyl disulfide of the corresponding stable cations and characterized by neutralization–reionization mass spectrometry and ab initio calculations. Hypervalent radical **1** dissociates extensively by losses of hydrogen and methyl, which are calculated to be exothermic by 69 and 103 kJ mol⁻¹, respectively. A small fraction (~0.5%) of **1** is metastable and survives for 3.7 μs to be detected as stable ions after collisional reionization with oxygen. An unusual inverse deuterium isotope effect on dissociations of **1** is found that stabilizes $(CH_3)_3NH^•$ and $(CHD_2)(CH_3)_2$-$NH^•$ against $(CH_3)_3ND^•$. MP2(FULL)/6-31+G(d) calculations find a very shallow potential energy minimum for the $^2A_1$ electronic ground state of **1**, which is predicted to dissociate completely by loss of hydrogen. A potential energy barrier is found for the loss of methyl from the $^2A_1$ ground state of **1**. The existence of metastable **1** and the methyl loss are explained by low-lying bound excited states which are accessed on collisional neutralization.

Introduction

One-electron reduction of first-row onium cations produces radicals that have formally nine valence electrons at the central atom and thus violate the octet rule.[1,2] Hypervalent radicals of the XH_n type, e.g., $H_3^•$,[3] $H_3O^•$,[4] and $NH_4^•$,[5] have been of much theoretical interest,[6] sparked by gas-phase studies that generated these species by collisional neutralization of fast onium ions with thermal atoms or molecules.[7] Dissociations of hypervalent radicals exhibit unusually large isotope effects that often make possible observations of metastable $XD_n^•$ of microsecond lifetimes, whereas the protonated analogs dissociate completely on the same time scale.[7]

Simple organic hypervalent radicals of the onium type, e.g., $CH_3NH_3^•$,[7b] $CH_3OH_2^•$,[8a] $(CH_3)_2OH^•$,[8b,c] and $CH_3CH_2OH_2^•$,[8c,d] have been generated by neutralization of the corresponding gaseous cations and characterized by neutralization–reionization

mass spectrometry.[9] These radicals also show very large isotope effects stabilizing the isotopomers with N–D or O–D bonds; in addition, inverse isotope effects have been noted in the dissociations of $CD_3CD_2OD_2^•$, which is kinetically less stable than CH_3CH_2-$OD_2^•$.[8c] By contrast, deuterium isotope effects appear to be much smaller in dissociations of hypervalent radicals derived from second-row atoms, e.g., $(CH_3)_2S^•OH$,[10a,b] and $P^•(OH)_4$.[10c]

A conspicuous feature of the dissociations of hypervalent ammonium and oxonium radicals is the occurrence of both X–C and X–H (X = N, O) bond cleavages which take place in spite of large differences in the corresponding reaction enthalpies. For example, the O–C bond cleavage in $(CH_3)_2OH^•$ is 90 kJ mol⁻¹ more exothermic than the O–H bond cleavage,[11,12] and a similar trend is encountered with dissociations of N–C and N–H bonds in hypervalent ammonium radicals. These parallel bond cleavages raise the question of activation energies in the dissociations of metastable hypervalent radicals and the involvement of vibrationally and electronically excited states.[4c,5]

In this paper we report on the preparation of the first fully protonated metastable hypervalent ammonium radical, $(CH_3)_3$-$NH^•$, **1**, and inverse deuterium isotope effects on its dissociations, as studied for $(CHD_2)(CH_3)_2N^•H$ (**1a**) and $(CH_3)_3N^•D$ (**1b**). Ab initio calculations are used to investigate the electronic structure of **1** and the potential energy profiles along the dissociation paths for losses of methyl and hydrogen.

Experimental Section

Neutralization–reionization ($^+NR^+$) spectra were obtained on a tandem quadrupole acceleration–deceleration mass spectrometer described previously.[13] $(CH_3)_2NH^{•+}$, $(CH_3)_3N^{•+}$, and $(CHD_2)(CH_3)N^{•+}$ precursor ions were generated by electron impact ionization (70 eV, emission current 500 μA) of the corresponding stable molecules. $(CH_3)_3NH^+$ (**1⁺**) was

⊕ Abstract published in *Advance ACS Abstracts,* September 1, 1994.

(1) Lewis, G. N. *J. Am. Chem. Soc.* **1916,** *38,* 762–785.

(2) Reed, A. E.; Schleyer, P. v. R. *J. Am. Chem. Soc.* **1990,** *112,* 1434–1445.

(3) Gellene, G. I.; Porter, R. F. *Acc. Chem. Res.* **1990,** *23,* 141–147 and references cited therein.

(4) (a) Niblaeus, K. S. E.; Roos, B. O.; Siegbahn, P. E. M. *Chem. Phys.* **1977,** *25,* 207–213. (b) Talbi, D.; Saxon, R. P. *J. Chem. Phys.* **1989,** *91,* 2376–2387. (c) McLoughlin, P. W.; Gellene, G. I. *J. Phys. Chem.* **1992,** *96,* 4396–4404.

(5) (a) McMaster, B. N.; Mrozek, J.; Smith, V. H. *Chem. Phys.* **1982,** *73,* 131–143. (b) Cardy, H.; Liotard, D.; Dargelos, A.; Poquet, E. *Chem. Phys.* **1983,** *77,* 287–299. (c) Kaspar, J.; Smith, V. H.; McMaster, B. N. *Chem. Phys.* **1985,** *96,* 81–95. (d) Kassab, E.; Evleth, E. M. *J. Am. Chem. Soc.* **1987,** *109,* 1653–1661.

(6) Demolliens, A.; Eisenstein, O.; Hiberty, P. C.; Lefour, J. M.; Ohanessian, G.; Shaik, S. S.; Volatron, F. *J. Am. Chem. Soc.* **1989,** *111,* 5623–5631.

(7) (a) Williams, B. W.; Porter, R. F. *J. Chem. Phys.* **1980,** *73,* 5598–5604. (b) Gellene, G. I.; Cleary, D. A.; Porter, R. F. *J. Chem. Phys.* **1982,** *77,* 3471–3477. (c) Gellene, G. I.; Porter, R. F. *Acc. Chem. Res.* **1983,** *16,* 200–207. (d) Gellene, G. I.; Porter, R. F. *J. Chem. Phys.* **1984,** *81,* 5570–5576. (e) Gellene, G. I.; Porter, R. F. *J. Phys. Chem.* **1984,** *88,* 6680–6684. (f) Jeon, S.-J.; Raksit, A. B.; Gellene, G. I.; Porter, R. F. *J. Am. Chem. Soc.* **1985,** *107,* 4129–4133. (g) Wesdemiotis, C.; Feng, R.; McLafferty, F. W. *J. Am. Chem. Soc.* **1986,** *108,* 5656–5657. (h) Gellene, G. I.; Porter, R. F. *Int. J. Mass Spectrom. Ion Processes* **1985,** *64,* 55–66. (i) Raksit, A. B.; Porter, R. F. *Int. J. Mass Spectrom. Ion Processes* **1987,** *76,* 299–306. (j) Hudgins, D. M.; Porter, R. F. *Int. J. Mass Spectrom. Ion Processes* **1994,** *130,* 49–64.

(8) (a) Raksit, A. B.; Porter, R. F. *Org. Mass Spectrom.* **1987,** *22,* 410–417. (b) Holmes, J. L.; Sirois, M. *Org. Mass Spectrom.* **1990,** *25,* 481–482. (c) Sirois, M.; George, M.; Holmes, J. L. *Org. Mass Spectrom.* **1994,** *29,* 11–17. (d) Wesdemiotis, C.; Fura, A.; McLafferty, F. W. *J. Am. Soc. Mass Spectrom.* **1991,** *2,* 459–463.

(9) (a) Danis, P. O.; Wesdemiotis, C.; McLafferty, F. W. *J. Am. Chem. Soc.* **1983,** *105,* 7454–7456. For recent reviews, see: (b) Holmes, J. L. *Mass Spectrom. Rev.* **1989,** *8,* 513–539. (c) McLafferty, F. W. *Science (Washington, D.C.)* **1990,** *247,* 925–929.

(10) (a) Gu, M.; Tureček, F. *J. Am. Chem. Soc.* **1992,** *114,* 7146–7151. (b) Tureček, F. *Org. Mass Spectrom.* **1992,** *27,* 1087–1097. (c) Tureček, F.; Gu, M.; Hop, C. E. C. A. *J. Phys. Chem.,* submitted for publication.

(11) From the heats of formation (kJ mol⁻¹) of H (218), CH₃ (146), CH₃OH (−202), and (CH₃)₂O (−184); see ref 12.

(12) Lias, S. G.; Bartmess, J. E.; Liebman, J. F.; Holmes, J. L.; Levin, R. D.; Mallard, W. G. *J. Phys. Chem. Ref. Data, Suppl. 1* **1988,** *17,* 134.

(13) Tureček, F.; Gu, M.; Shaffer, S. A. *J. Am. Soc. Mass Spectrom.* **1992,** *3,* 493–501.

Table 1. Total Energies Calculated with the 6-31 + G(d) Basis Set

species	energy[a]					
	HF	MP2[b]	MP4(SDTQ)[b]	MP2(FULL)	ZPVE[c]	ΔH_{298}[d]
1+	-173.651 613	-174.209 132	-174.276 526	-174.228 451	342.1	17.5
1+(VI)[e]	-173.648 663	-174.207 567	-174.274 801		333.9	
1	-173.741 599	-174.316 905	-174.384 881	-174.337 387	333.9	17.5
1(VN)[f]	-173.739 549	-174.313 236	-174.381 700	-174.333 759	342.1	
TS(N--H)[g]	-173.737 412	-174.317 219	-174.384 578	-174.336 336	315.6	17.8
(CH3)2NH--CH3[h]	-173.711 527					
(CH3)3N	-173.272 906	-173.838 453	-174.903 844		303.7	17.1
(CH3)2NH	-134.242 641	-134.673 944	-134.723 440		232.5	14.3
CH3•	-39.561 101	-39.672 303	-39.692 957	-39.676 728	73.2	11.1
H•	-0.498 233					6.2

[a] Hartrees; 1 hartree = 2625.5 kJ mol⁻¹. $\langle S^2 \rangle$ values were within 0.75-0.752 for all UHF calculations. [b] Single-point calculations on HF/6-31 + G(d) optimized geometries. MP3 energies showed convergence of the MP series. [c] From 6-31 + G(d) harmonic frequencies scaled by 0.89, kJ mol⁻¹. [d] Enthalpy corrections for $H_{298} - H_0$, kJ mol⁻¹. [e] From vertical ionization of 1. [f] From vertical neutralization of 1+. [g] Transition state for the N-H bond dissociation in 1. [h] At a C-N bond length of 1.78 Å.

prepared by gas-phase protonation of $(CH_3)_3N$ with $C_4H_9^+$, NH_4^+ and H_3O^+. $(CHD_2)(CH_3)_2NH^+$ (**1a+**) was prepared by protonation of $(CHD_2)(CH_3)_2N$ with $C_4H_9^+$. $(CH_3)_3ND^+$ (**1b+**) was prepared by protonation with $C_4D_9^+$ generated by chemical ionization (CI) of $(CD_3)_3$-CD (MSD Isotopes, 99% D). The ion source and gas inlet walls were conditioned with D_2O at 2×10^{-5} Torr for 1 h prior to the deuteronation experiments. Chemical ionization was carried out in a tight ion source of our design. The reagent gas pressure and ion source potentials were adjusted to optimize protonation and minimize electron ionization of the amines so as to obtain ion abundance ratios of $[M + H]^+/[M^{+}] > 20$. Typical ionization conditions were as follows: reagent gas pressure, 2×10^{-4} Torr as read on an ionization gauge mounted at the diffusion pump intake; emission current, 1 mA; source temperature, 180 °C. The precursor ions were passed through a quadrupole mass filter, accelerated to 8200 eV, and neutralized by collisions with gaseous CH_3SSCH_3 or $(CH_3)_3N$ at pressures such as to achieve 70% transmittance of the precursor ion beam. The time between ion formation and neutralization is estimated from ion trajectory calculations as 130 μs for m/z 60. Hence stable, long-lived ions were sampled for collisional neutralization. The remaining ions were separated electrostatically from the neutral products,[13] and the latter were reionized after 3.7 μs by collisions with oxygen at 70% transmittance of the precursor ion beam. Collisionally activated dissociation (CAD) of the intermediate neutrals was carried out by admitting helium in the differentially pumped neutral drift region[13,14] at a pressure such as to achieve 50% transmittance of the precursor ion beam. The drift region was floated at +250 V, so that any ions formed there had kiloelectronvolt total energies and were rejected by an energy filter.[13,14] The spectra were obtained by linked scanning of the deceleration potential and the second quadrupole mass analyzer to provide both precursor and product mass separation.[13,14] The reported spectra were averaged over 25-30 repetitive scans obtained at scan rates of 1 s (75 data points) per mass unit. The spectra of $(CH_3)_3NH^\bullet$ were measured in six runs over a period of several months. The CAD spectrum of **1+** at 4 keV kinetic energy was measured on a Kratos Profile HV-4 double-focusing mass spectrometer as described previously.[14] Dimethylamine and trimethylamine (both Matheson, 99.9%) were used as received. Dimethyl(methyl-d_2)amine was synthesized by LiAlD₄ (Aldrich, 98% d) reduction of dimethylformamide in tetrahydrofuran and purified by vacuum distillation.

Calculations

Standard ab initio calculations were carried out using the GAUSSIAN 92 program package.[15] Geometries in the trimethylamine system were optimized with the 6-31+G(d) basis set to obtain potential energy minima (all frequencies real) and first-order saddle points (one imaginary frequency). Zero-point vibrational energies and 298 K enthalpies were obtained from the harmonic vibrational frequencies (available as supplementary

(14) Shaffer, S A.; Turecek, F.; Cerny, R. L. *J. Am. Chem. Soc.* **1993,** *115,* 12117-12124.

(15) Gaussian 92, Revision C; Frisch, M. J.; Trucks, G. W.; Head-Gordon, M.; Gill, P. M. W.; Wong, M. W.; Foresman, J. B.; Johnson, B. G.; Schlegel, H. B.; Robb, M. A.; Replogle, E. S.; Gomperts, R.; Andres, J. L.; Raghavachari, K.; Binkley, J. S.; Gonzalez, C.; Martin, R. L.; Fox, D. J.; DeFrees, D. J.; Baker, J.; Stewart, J. J. P.; Pople, J. A. Gaussian, Inc. Pittsburgh, PA, 1992.

material) scaled by 0.89.[16] No symmetry constraints were used in the initial optimizations; the structures that implied molecular symmetry were reoptimized with symmetry constraints using the 6-31+G(d) basis set. The structures of **1**, **1+**, and several points on the dissociation paths for loss of hydrogen and methyl were further reoptimized with the 6-31+G(d) basis set including perturbational Møller-Plesset treatment[17] of electron correlation effects truncated at second-order (MP2(FULL)).[15] Improved energies were obtained from single-point calculations on the HF/6-31+G(d) optimized geometries using the Møller-Plesset theory[17] (frozen core) truncated at fourth order with single, double, and triple excitations (MP4(SDTQ)). Effects of limited basis size were examined with MP2(frozen core) single-point calculations using the larger 6-31++G(d,p) basis set. The geometries in the ammonium system were optimized with UHF/6-31++G-(d,p) calculations and reoptimized with MP2(FULL)/6-31++G-(d,p). The latter geometries were used for single-point MP4-(SDTQ) calculations. In all cases, the MP2, MP3, and MP4 energies converged. To obtain energies of the doublet excited states of **1**, the electron was promoted from the SOMO ($7a_1$) to one of the lowest virtual orbitals (7e, 8e), and the UHF wave functions were calculated with frozen C_{3v} molecular geometry. Contamination from higher spin states was negligible in the spin-unrestricted calculations as judged from the $\langle S^2 \rangle$ values, which ranged within 0.75-0.752. The calculated total energies are summarized in Tables 1 and 2; the relative energies are given in Table 3.

Results and Discussion

Formation of $(CH_3)_3N^\bullet H$, $(CH_3)_3N^\bullet D$, and $(CHD_2)(CH_3)_2N^\bullet H$. The stable $(CH_3)_3NH^+$ ion (**1+**) was prepared by gas-phase protonation of trimethylamine and used to generate the hypervalent radical **1** (Scheme 1). Ion **1+** was characterized by its collisionally activated dissociation (CAD) spectrum (Figure 1a), which shows major fragments due to loss of H (m/z 59), CH_3 (m/z 45), methane (m/z 44), $HCNH^+$ (m/z 28), and CH_3^+ (m/z 15). Collisional neutralization of stable **1+** followed by reionization results in extensive dissociation (Figure 1b). The fragments observed, m/z 45, 44, 28, 13-15, and m/z 59, 58, 42, 26-28, 13-15, also dominate the $^+NR^+$ spectra of $(CH_3)_2NH^{\bullet+}$ (Figure 2a) and $(CH_3)_3N^{\bullet+}$ (Figure 2b), respectively, and provide evidence of the intermediacy of neutral trimethylamine and dimethylamine. This indicates that **1** dissociates primarily by N-C and N-H bond cleavages, and the neutral products and their reionized counterparts then undergo further dissociations.

A conspicuous feature of the $^+NR^+$ spectrum of **1+** is the presence of a small but significant survivor ion at m/z 60. The relative abundance of the survivor ion **1+** (0.5% of the total

(16) Curtiss, L. A.; Raghavachari, K.; Pople, J. A. *J. Chem. Phys.* **1993,** *98,* 1293-1298.

(17) Møller, C.; Plesset, M. S. *Phys. Rev.* **1934,** *46,* 618-622.

Table 2. Total Energies Calculated with the 6-31++G(d,p) Basis Set
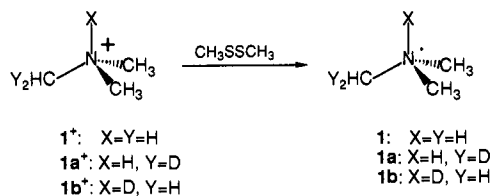
species	molecular symmetry	UHF	MP2(FULL)	MP2[a]	MP4(SDTQ)[a,b]	ZPVE[c]	ΔH_{298}
NH$_4^•$	T_d	−56.693 664	−56.899 695	−56.895 776	−56.916 425	116	10.0
TS(NH$_3$- -H)	C_{3v}	−56.668 112	−56.876 309	−56.872 505	−56.892 610	94	10.6
1(^{2}A$_1$)	C_{3v}	−173.772 050					
		−173.771 826[d]		−174.406 441[d]			
1(7e)[1]	C_{3v}	−173.731 283[d]					
TS(N- -H)	C_{3v}	−173.761 742[d]		−174.402 757[d]			
(CH$_3$)$_2$NH- -CH$_3^e$	C_s	−173.743 171[d]		−174.380 537[d]			

[a] Single-point calculations on MP2(FULL) optimized geometries. NH$_4^•$: r(N–H) = 1.037 Å, $\angle$(HNH) = 109.5°. TS(NH$_3$- -H(4)): r(N–H(4)) = 1.435 Å, r(N–H) = 1.018 Å, $\angle$(HNH) = 109.4°, $\angle$(H(4)NH) = 109.5°, $\angle$(HNHH) = 119.9°, $\angle$(H(4)–NHH) = 120.2°. [b] The MP2, MP3, and MP4 total energies converged. [c] From UHF/6-31++G(d,p) harmonic frequencies scaled by 0.89, kJ mol^{-1}. [d] Single-point calculations on UHF/6-31 + G(d) optimized geometries. [e] At an N–C bond length of 1.78 Å.

Table 3. Relative Energies

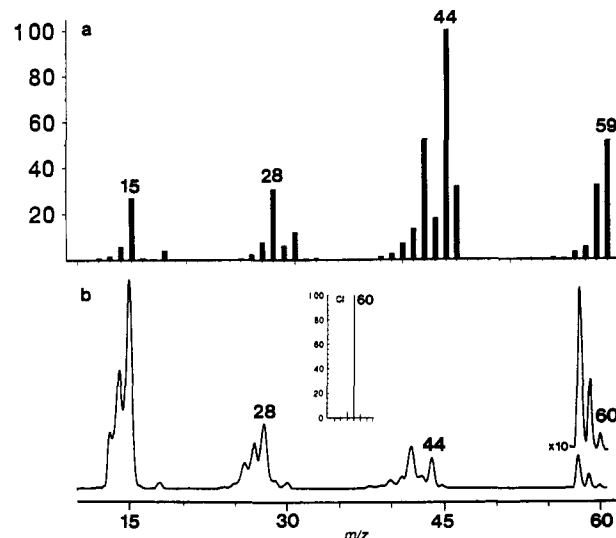|	relative energy[a]		
species	MP2	MP4	MP2(FULL)
1	0	0	0
1(VN)[b]	17.8	16.6	17.7
1$^+$	291 (3.02)[c]	293 (3.03)[c]	294 (3.05)[c]
1$^+$(VI)[d]	287 (2.98)[e]	289 (3.00)[e]	
(CH$_3$)$_3$N + H$^•$	−76	−69	
TS(N- -H)[f]	−18(−8)[g]	−17	−15
(CH$_3$)$_2$NH + CH$_3^•$	−97	−103	
NH$_4^•$ [h]	0	0	0
TS(NH$_3$- -H)[h]	40	41	40

[a] Including ZPVE and 298 K enthalpy corrections, kJ mol^{-1}. [b] From vertical neutralization of 1$^+$. [c] Adiabatic ionization energies in eV. [d] From vertical ionization of 1. [e] Vertical ionization energies in eV. [f] Transition state for the N–H bond dissociation in 1. [g] From MP2/6-31++G(d,p) calculations. [h] Calculations with the 6-31++G(d,p) basis set (Table 2).

Scheme 1

1$^+$: X=Y=H
1a$^+$: X=H, Y=D
1b$^+$: X=D, Y=H

1: X=Y=H
1a: X=H, Y=D
1b: X=D, Y=H

Figure 1. (a) Collisionally activated dissociation spectrum of 1$^+$ (O$_2$, 70% ion beam transmittance). (b) $^+$NR$^+$ spectrum of 1$^+$ (CH$_3$SSCH$_3$, 70% transmittance/O$_2$, 70% transmittance). Inset: (M + H)$^+$ region in the CI/C$_4$H$_9^+$ spectrum.

reionized ion current, Σ^+NR$^+$, in Figure 1b) showed small variations in measurements carried out over the period of several months with an average of 0.4 ± 0.1% Σ^+NR$^+$. Careful analysis of precursor ion intensities at adjacent m/z shows that the reionized ion intensity at m/z 60 in the $^+$NR$^+$ spectrum cannot be accounted for by interferences from isobaric overlaps, e.g., from ^{13}C and ^{15}N isotopomers of residual (CH$_3$)$_3$N$^{•+}$ coformed with 1$^+$ in the ion source. It follows from the measured $^+$NR$^+$ yields and ion relative abundances that only ~7% of the ion intensity at m/z 60 can be attributed to interfering ion species,[18] while the major part is due to reionization of surviving hypervalent radical 1. The relative intensity of survivor 1$^+$ was found to depend on the protonation exothermicity and ion source temperature. The highest relative abundance of survivor 1$^+$ was obtained from 1$^+$ formed by exothermic protonation of (CH$_3$)$_3$N with C$_4$H$_9^+$ (ΔPA = 148 kJ mol^{-1})[19] and neutralized with CH$_3$-SSCH$_3$. Less exothermic protonation with NH$_4^+$ (ΔPA = 99 kJ mol^{-1})[19] or more exothermic protonation with H$_3$O$^+$ (ΔPA = 260

(18) (CH$_3$)$_3$N: $\Sigma[^+$NR$^+]/[$precursor m/z 59] = 0.0040; [reionized m/z 59]/$\Sigma[^+$NR$^+]$ = 0.102; [reionized m/z 59]/[precursor m/z 59] = 4.08 × 10^{-4}. For the precursor ion ratio in the CI spectrum, [m/z 59]/[m/z 60] = 0.0417, the contribution of (CH$_3$)$_3$N ^{13}C and ^{15}N isotopomers at m/z 60 is 0.147%. Presuming the same $^+$NR$^+$ yields for all isotopomers of (CH$_3$)$_3$N gives [reionized m/z 60]/[precursor m/z 60] = 0.001 47 × 4.08 × 10^{-4} = 6.1 × 10^{-7}. For 1$^+$, $\Sigma[^+$NR$^+]/[$precursor m/z 60] = 0.0016, [reionized m/z 60]/$\Sigma[^+$NR$^+]$ = 0.0055, [reionized m/z 60]/[precursor m/z 60] = 8.8 × 10^{-6}. The contribution at m/z 60 of ^{13}C and ^{15}N isotopomers of (CH$_3$)$_3$N in the $^+$NR$^+$ spectrum of 1$^+$ is therefore 6.1 × 10^{-7}/8.8 × 10^{-6} or 7%.

(19) From the revised proton affinities (kJ mol^{-1}) of (CH$_3$)$_3$N (950), C$_4$H$_8$ (802), NH$_3$ (851.4), and H$_2$O (690); see ref 12 and the following: (a) Szulejko, J. E.; McMahon, T. B. *J. Am. Chem. Soc.* **1993**, *115*, 7839–7848. (b) Meot-Ner (Mautner), M.; Sieck, L. W. *J. Am. Chem. Soc.* **1991**, *113*, 4448–4460.
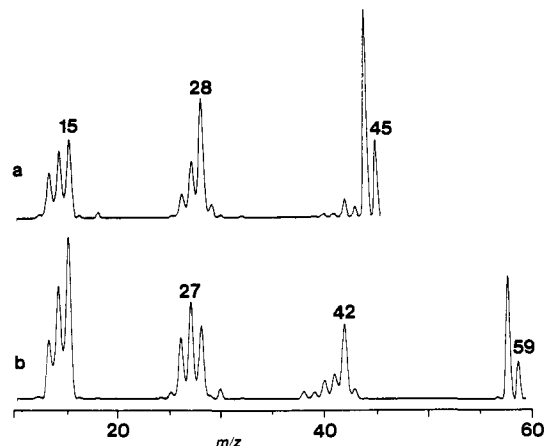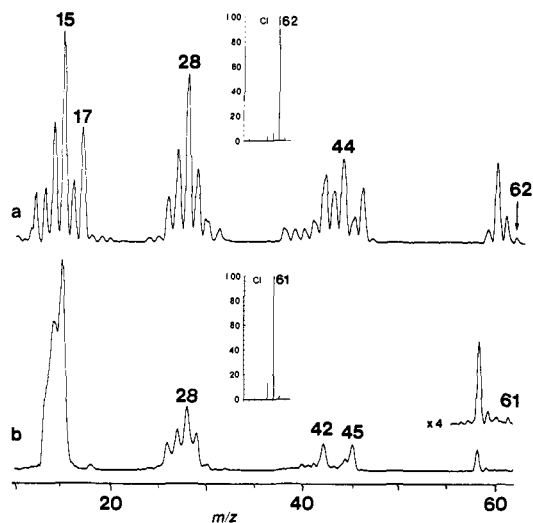
Figure 2. $^+$NR$^+$ spectra (CH$_3$SSCH$_3$, 70% T/O$_2$, 70% T) of (a) (CH$_3$)$_2$-NH$^{•+}$ and (b) (CH$_3$)$_3$N$^{•+}$.

kJ mol^{-1})[19] resulted in lower relative abundances of survivor 1$^+$ following neutralization with CH$_3$SSCH$_3$ and reionization with O$_2$ (0.2 and 0.1% $\Sigma[^+$NR$^+]$, respectively). Neutralization with (CH$_3$)$_3$N of C$_4$H$_9^+$-protonated 1$^+$ gave 0.35% $\Sigma[^+$NR$^+]$ survivor 1$^+$ after reionization with O$_2$, which is comparable to the result from neutralization with CH$_3$SSCH$_3$.

Temperature dependence of the survivor 1$^+$ relative abundance was examined for ion sources temperatures in the 140–200 °C range and isobutane pressures such as to achieve quantitative formation of 1$^+$; the precursor ion was neutralized with CH$_3$-SSCH$_3$ and reionized with O$_2$ in these measurements. The peak of survivor 1$^+$ is maximized at around 180 °C and decreases

Figure 3. $^+NR^+$ spectra (CH₃SSCH₃, 70% T/O₂, 70% T) of (a) (CHD₂)(CH₃)₂NH⁺ and (b) (CH₃)₃ND⁺. Insets: (M + H,D)⁺ regions in the CI mass spectra.

Figure 4. $^+NR^+$ (CH₃SSCH₃, 70% T/O₂, 70% T) (top) and $^+NCR^+$ (CH₃SSCH₃, 70% T/He, 50% T/O₂, 70% T) (bottom) spectra of (CHD₂)-(CH₃)₂N$^{•+}$.

toward lower or higher ion source temperatures. At 140 and 200 °C the peak of survivor 1⁺ falls below 0.1% Σ[⁺NR⁺], and its intensity fluctuates and becomes poorly reproducible. This indicates that the kinetically metastable 1 is formed as a small fraction of total 1 which is affected by the precursor ion internal energy. The cause of the temperature dependence is not clear; within the temperature range used the average thermal energies of (CH₃)₃N and (CH₃)₃NH⁺ change by only 7.4 and 7.8 kJ mol⁻¹,[20] respectively, which is small compared with the width of the vibrational energy distribution.[21] We have not attempted any pressure dependence studies analogous to those reported for (CH₃)₂OH⁺ and CH₃CH₂OH₂⁺,[8b,c] as the interferences from the much more efficient neutralization of (CH₃)₃N isotopomers present under low-pressure conditions would render identification of survivor 1⁺ unreliable.

Similar to 1⁺, neutralization–reionization of its methyl-labeled analog 1a⁺ gives a significant survivor ion at m/z 62 (0.4% Σ[⁺NR⁺], Figure 3a). Corrections for the contributions of ¹³C and ¹⁵N isotopomers amount to only 9% relative intensity at m/z 62, confirming that the ion is predominantly formed by reionization of hypervalent 1a. However, in contrast to 1⁺ and 1a⁺, neutralization–reionization of the N–D-labeled ion 1b⁺ gives a very weak survivor ion (0.15% Σ[⁺NR⁺], Figure 3b), a part of which is due to the ¹³C and ¹⁵N contributions from the accompanying (M + D − H)⁺ ion. This contrasts the previous observations of organic hypervalent radicals whose oxygen- or nitrogen-deuterated derivatives were substantially more stable than the protonated forms.[8]

The competing losses of hydrogen and methyl from hypervalent 1 and its isotopomers deserve some comment. Loss of methyl gives rise to (CH₃)₂NH and its isotopomers, which nevertheless appear as small peaks in the ⁺NR⁺ spectra of 1⁺, 1a⁺, and 1b⁺ (Figures 1b and 3). By comparison, the ⁺NR⁺ spectrum of (CH₃)₂NH$^{•+}$ shows a substantial survivor ion (Figure 2a), whose main dissociation is loss of hydrogen to give C₂H₆N⁺ at m/z 44. The very low abundance of (MH − CH₃)⁺, and hence low [m/z 45]/[m/z 44], [m/z 47]/[m/z 46], and [m/z 46]/[m/z 45] ratios in the ⁺NR⁺ spectra of 1⁺, 1a⁺, and 1b⁺, respectively, can be explained by further dissociations of the (CH₃)₂NH neutral and, especially, the (CH₃)₂NH$^{•+}$ ion formed therefrom. Ion and neutral heats of formation[12] show much smaller endothermicities
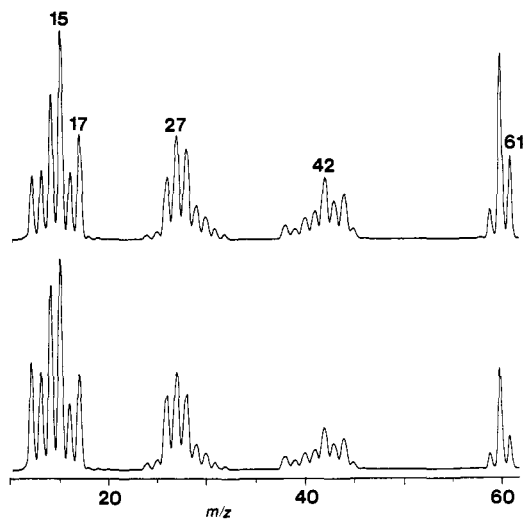
for ion dissociations; for example, (CH₃)₂NH$^{•+}$ → CH₂=NH⁺-CH₃ + H$^•$ requires 137 kJ mol⁻¹, whereas simple cleavages in neutral (CH₃)₂NH of C–H, N–H, and N–C bonds require 362, 381, and 350 kJ mol⁻¹, respectively.[12] Hence, (CH₃)₂NH formed from hypervalent 1 by loss of methyl with up to ~350 kJ mol⁻¹ internal energy will survive as a neutral molecule, but its cation radical will dissociate by loss of hydrogen following reionization. Consistent with this, endothermic neutralization of (CH₃)₂NH$^{•+}$ with xenon (ΔIE$_v$ = −3.16 eV),[22] which presumably leads to energy deposition in the (CH₃)₂NH formed,[9b] results in more extensive dissociation giving [m/z 45]/[m/z 44] = 0.2 as compared with 0.4 from the near-resonant neutralization with CH₃SSCH₃ (ΔIE$_v$ = 0.01 eV)[22] (Figure 2a).

The complementary CH₃⁺ ion and its dissociation products dominate the ⁺NR⁺ spectra of 1⁺ and 1b⁺, and the spectrum of 1a⁺ shows dominant CH₃⁺ and CHD₂⁺ in an approximately statistical 2:1 ratio (Figure 3a). The high abundance of the methyl fragments is indicative of N–C bond cleavage dissociations in 1, but in part is also due to subsequent dissociations of the primary (CH₃)₃N and (CH₃)₂NH products as neutral molecules and/or reionized ions. Consistent with this, the substantial relative abundance of (C,H,D)⁺ fragments in the ⁺NR⁺ spectrum of (CHD₂)(CH₃)₂N$^{•+}$ (43.2% Σ[⁺NR⁺]) further increases to 55% Σ[⁺NR⁺] on collisional activation of the intermediate neutrals (Figure 4).

To summarize, the spectral data point to a small fraction of kinetically metastable 1 and 1a that survive for 3.7 μs and are detected after collisional reionization. The presence of deuterium at N in 1b decreases the fraction of surviving radicals, indicating an inverse deuterium isotope effect on their dissociations.

Ab Initio Calculations. In order to rationalize the experimental results and gain some insight into the properties of 1, we investigated its stability and dissociation paths by ab initio calculations. Both the ground and the excited electronic states are likely to be important in the dissociations of 1.[8c,23] While the ground electronic state of 1 is investigated in detail here, potential energy mapping of the excited states would require multireference calculations[5c,d,24] which are beyond our capabilities for a system of this size. Hence relevant excited states of 1 are discussed only qualitatively.

(20) From the calculated harmonic frequencies and the rigid rotor-harmonic oscillator approximation.

(21) The calculated half-widths for the vibrational energy distribution in trimethylamine were 36 and 43 kJ mol⁻¹ at 413 and 473 K, respectively; see: Ehrhardt, H.; Osberghaus, O. *Z. Naturforsch.* **1960**, *15A*, 575.

(22) Kimura, K.; Katsumata, S.; Achiba, Y.; Yamazaki, T.; Iwata, S. *Handbook of He(I) Photoelectron Spectra of Fundamental Organic Molecules*; Japan Scientific Societies Press: Tokyo, 1981; pp 120, 214.

(23) (a) Yates, B. F.; Bouma, W. J.; Radom, L. *J. Am. Chem. Soc.* **1984**, *106*, 5805–5808. (b) Wesdemiotis, C.; Feng, R.; Danis, P. O.; Williams, E. R.; McLafferty, F. W. *J. Am. Chem. Soc.* **1986**, *108*, 5847–5853.

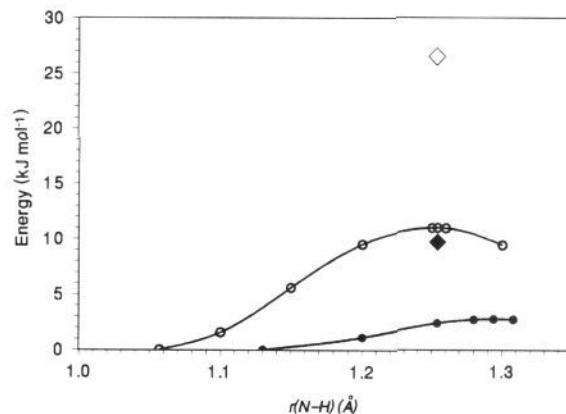(24) Roos, B. O. *Adv. Chem. Phys.* **1987**, *69*, 399.
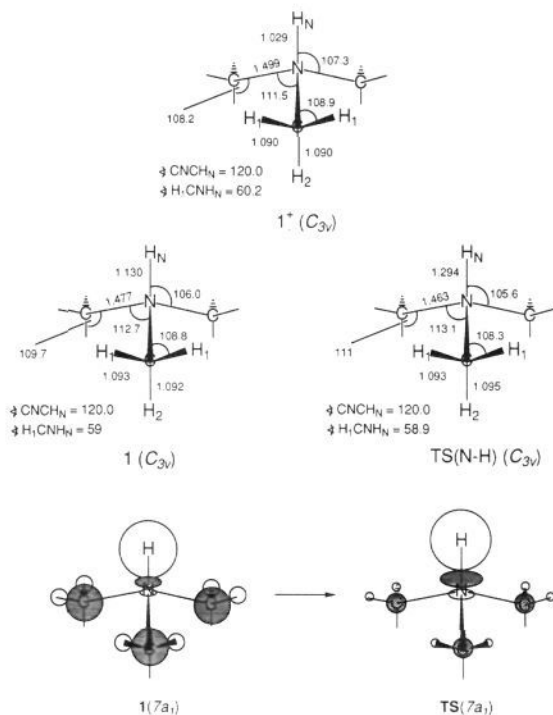
Figure 5. MP2(FULL)/6-31+G(d) optimized geometries of **1⁺**, **1**, and **TS(N–H)** and the singly occupied molecular orbitals.

Figure 6. Potential energy profile along the N–H coordinate in **1**. Empty circles: UHF/6-31+G(d) calculations. Solid circles: MP2(FULL)/6-31+G(d) calculations. Empty diamond: single-point UHF/6-31++G-(d,p) calculation. Solid diamond: single-point MP2/6-31++G(d,p) calculation.

Figure 7. Potential energy profile along the N–C coordinate in **1**. Empty circles: UHF/6-31+G(d) calculations. Solid circle: single-point MP2/6-31++G(d,p) calculation.

Geometry optimizations with the UHF/6-31+G(d), UHF/6-31++G(d,p), and MP2(FULL)/6-31+G(d) calculations find energy minima for the $^2A_1$ ground state of **1** (Figure 5). The equilibrium geometry of **1** is similar to that of ion **1⁺**, with the most significant difference being in the N–H bond length which is greater in the radical. Consequently, **1** and **1⁺** show different N–H vibrational frequencies, 2298 and 3326 cm⁻¹, respectively, indicating a much weaker N–H bond in the radical. The optimized N–H bond length depends slightly on the basis set used, e.g., 1.057 and 1.040 Å for the UHF/6-31+G(d) and 6-31++G(d,p) calculations, respectively, while the other bond lengths and angles are similar within 0.4% (see supplementary material).

In order to assess the kinetic stability of **1**, the reaction paths for the N–H and N–C bond dissociations were investigated. At the UHF/6-31+G(d) level, stretching the N–H bond overcomes a 11 kJ mol⁻¹ potential energy barrier resulting in an early transition state (Figure 6). MP2(FULL)/6-31+G(d) optimizations and MP4//MP2(FULL) single-point calculations lead to even lower potential energy barriers (2.8 and 0.8 kJ mol⁻¹, Figure 6), while a single-point MP2/6-31++G(d,p) calculation gives 9.7 kJ mol⁻¹ (Figure 6). These small differences in the calculated potential energy barriers are overwhelmed by the decrease in the zero-point vibrational energy from **1** to **TS(N–H)**, ΔZPVE = –18 kJ mol⁻¹, which makes the hypervalent radical dynamically unstable. Hence on formation ($^2A_1$) **1** is predicted to dissociate exothermically (ΔH_r = –69 kJ mol⁻¹, Table 3) and *without a barrier* to (CH₃)₃NH and H.

A different potential energy profile is found for the N–C bond dissociation path. Stretching one of the N–C bonds in **1** results in a significant rise of potential energy as shown in Figure 7 for the UHF/6-31+G(d) and MP2/6-31++G(d,p) calculations. The UHF potential energy surface shows a discontinuity at N–C bond lengths (r(N–C)) of 1.78–1.79 Å (Figure 7). It is tempting to assign this discontinuity to an avoided crossing of the ground potential energy surface with that of an excited state of E symmetry. However, the discontinuity may also be an artifact due to an inadequate description of the system by a single-determinant wave function in the region where the energy of the molecular orbital describing the dissociating bond approaches or
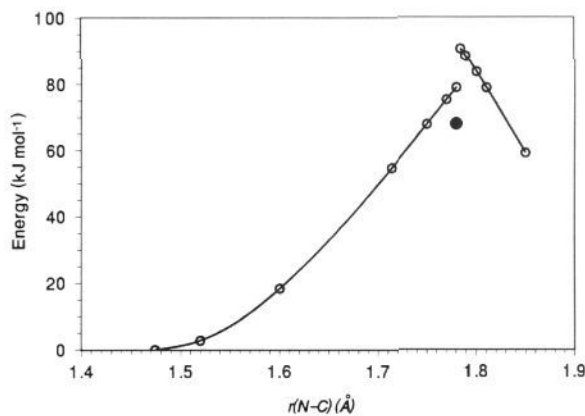
exceeds that of the SOMO. Multireference calculations[24] will be needed to clarify this point. As an approximation, an MP2 single-point calculation at r(N–C) = 1.78 Å shows a significant potential energy increase (Figure 7), suggesting a ≥60 kJ mol⁻¹ potential energy barrier for the loss of CH₃ in ($^2A_1$) **1**. It should be noted that the N–C bond dissociation is likely to involve a smaller change in the zero-point vibrational energy compared to that occurring in the N–H dissociation coordinate. Although the ZPVE change could not be calculated for the transition state, the points along the UHF calculated N–C coordinate show a gradual decrease of the N–H bond length from 1.058 Å in **1** through 1.039 at r(N–C) = 1.78 Å, up to 1.000 Å in (CH₃)₂NH. This N–H bond shortening results in an increase of the N–H stretching frequency from 2298 cm⁻¹ in **1** to 3357 cm⁻¹ in (CH₃)₂-NH to cause an increase in the ZPVE and compensate in part the loss of the N–C stretch in the transition state. It can be concluded that the $^2A_1$ state of **1** is bound with respect to the N–C bond cleavage, but dynamically unstable toward N–H bond dissociation.

Could vertical electron transfer destabilize the N–C mode through Franck–Condon effects? The equilibrium geometries of **1⁺** and **1** show only minor differences in the N–C bond lengths (Figure 5), which should cause very small excitation along the N–C coordinates (Figure 7), provided the neutralization occurred from the ground (all $v = 0$) vibrational state of **1⁺**. The calculated energy deposition in vertically formed **1** (17 kJ mol⁻¹ for the $v = 0$ transition, Table 3) can be attributed to the different N–H bond lengths in **1** and **1⁺** such that the former is produced with

a slightly compressed N–H bond on vertical neutralization. Due to the instability along the N–H coordinate, the compression should further promote N–H bond dissociation. A more intriguing situation arises in vertical neutralization of thermally excited 1^+. Although the 36 vibrational degrees of freedom in each 1^+ and 1 make a detailed analysis of the mode excitation[4c,5c] intractable, crude information can be obtained from the calculated harmonic vibrational frequencies of the precursor ion and 1. Presuming that ions 1^+ are formed at 453 K thermal equilibrium in the high-pressure ion source, most vibrational excitation should be localized in the low-frequency modes corresponding to methyl internal rotations (A_1, 181 cm^{-1}, and E, 247 cm^{-1}) and the C–N–C bending modes (E, 380 cm^{-1}, and A_1, 439 cm^{-1}), whereas the N–H stretching mode shows negligible excitation. The N–C skeletal stretching modes are only slightly excited; e.g., on average $\sim 10\%$ of the A_1 mode at 765 cm^{-1} and $\sim 5\%$ of the E modes at 943 cm^{-1} will be in the $v = 1$ states at 453 K. These crude estimates indicate that vertical neutralization of thermalized 1^+ should result in a relatively small vibrational excitation through Franck–Condon effects of the N–C stretching modes in 1, similar to the situation predicted for 0 K.

The calculations suggest that the behavior of 1 cannot be accounted for by the properties of the ground $^2A_1$ state alone. Since the ground state is dissociative with respect to N–H bond cleavage, the observed C–N bond cleavage and the small fraction of surviving 1 must come from one or more excited electronic states whose potential energy profiles differ from that of the $^2A_1$ state. Although a detailed investigation of potential energy surfaces for excited doublet states of 1 would require a multi-reference approach,[5d,24] some insight into the nature of the excited states can be achieved by qualitative analysis of the unoccupied orbitals in 1 obtained from Mulliken population analysis of the UHF wave function for the $^2A_1$ state.

To test the adequacy of the 6-31++G(d,p) basis set used,[25] we carried out pilot calculations of NH$_4^•$ ($^2A_1$, Table 2), for which multireference calculations incorporating sets of Rydberg orbitals are available for the ground[5c,d] and first three excited doublet states.[5d] The calculated depth of the potential energy minimum for ($^2A_1$) NH$_4^•$ (62 kJ mol^{-1} from MP4(SDTQ), Table 2) is in excellent agreement with that from the SDCI calculations of McMaster et al. (62 kJ mol^{-1})[5c] and in reasonable agreement with that from the CIPSI calculations of Kassab and Evleth (50 kJ mol^{-1}).[5d] The molecular orbitals in NH$_4^•$ closely correspond to the Rydberg orbitals of Kassab and Evleth,[5d] e.g., $3a_1 \leftrightarrow 3s$ (SOMO), $4t_2 \leftrightarrow 3p$, $4a_1 \leftrightarrow 4s$, and $5t_2 \leftrightarrow 4p$.[5d] Hence both the calculated energies and the orbital analysis in NH$_4^•$ indicate that the 6-31++g(d,p) basis set is adequate for describing the ground doublet state and a few lowest excited states in 1. Note that the far greater number of polarization and diffuse basis functions in 1 compared to that in NH$_4^•$ should result in an improved flexibility of the basis set, although higher angular-momentum Rydberg states may not be described properly with the basis set used.

Qualitatively, the instability of ($^2A_1$) 1 toward loss of hydrogen is due to the presence of the unpaired electron which enters the $7a_1$ orbital such that the electronic configuration in 1, $(1a_1)^2$-$(1e)^4(2a_1)^2(3e)^4(3a_1)^2(4a_1)^2(5a_1)^2(4e)^4(5e)^4(1a_2)^2(6e)^4(6a_1)^2$-$(7a_1)$, closely resembles that in 1^+, $(1a_1)^2(1e)^4(2a_1)^2(3a_1)^2(3e)^4$-$(4a_1)^2(5a_1)^2(4e)^4(5e)^4(1a_2)^2(6a_1)^2(6e)^4(7a_1)^0$. Figure 5 illustrates the dominant contribution of the hydrogen diffuse s orbital in the $7a_1$ SOMOs in both 1 and the transition state for hydrogen loss. In contrast to the $3a_1$ SOMO in NH$_4^•$, the $7a_1$ SOMO in 1 does not resemble a Rydberg 3s orbital, but rather can be described as a mixed valence–Rydberg p_z orbital.[26] The instability of the $^2A_1$ state could be attributed to the significant electron density at the nitrogen (-0.7) and the N-hydrogen atom (-0.21), and the
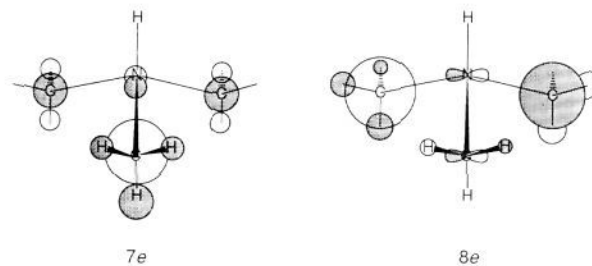

Figure 8. 7e and 8e unoccupied orbitals in 1.

antibonding character of the SOMO along the N–H bond. Similar features should characterize those excited states of 1 in which N–C bond cleavage is dominant or at least competitive with N–H bond dissociation. Such states, e.g., ^2E or atomic Rydberg states, should be orthogonal to the $^2A_1$ ground state to prevent fast electronic transition that would result in N–H bond dissociation. For example, electron capture in the 7e orbital (Figure 8) would create a ^2E state that, upon dissociation of the N–C bond, correlates with the electronic ground states of the products, $\tilde{X}^1A'(CH_3)_2NH$ and $\tilde{X}^2A_2''CH_3^•$.[27] Single-point calculations (Table 2) find the lowest ^2E states (7e and/or 8e SOMO) to be 1.1 eV above the $^2A_1$ ground state. Unfortunately, the potential energy profile in the ^2E states could not be calculated, because upon releasing the C_{3v} symmetry constraint to C_s the UHF wave functions collapsed to that of the $^2A_1$ state. Multireference calculations are clearly needed to obtain the depths and shapes of the potential wells in the ^2E states.

Assuming that some of the low-lying excited states in 1 are bound, one can explain the behavior of the radical upon neutralization. For example, the $(CH_3)_2NH$ formed by loss of methyl from the lowest-lying ^2E state of 1 will have a substantial internal energy (~ 200 kJ mol^{-1}, Tables 2 and 3) to promote dissociations of $(CH_3)_2NH^{•+}$ following reionization, as observed. Loss of methyl from a bound excited state of 1 can also provide rationalization of the inverse isotope effect observed for 1b. Upon stretching of the N–C bond in 1 the N–H bond becomes shorter to eventually achieve the standard bond length in the $(CH_3)_2NH$ product as discussed above for the $^2A_1$ state. Presuming that a similar effect occurs in the N–C dissociation proceeding on the excited state potential energy surface, the increased strength of the N–H bond in the transition state will result in its increased vibrational frequency which contributes to the zero-point vibrational energy. Since the increase in ZPVE in the transition state is greater in 1 than in 1b, the loss of methyl from the former must overcome a higher energy barrier, resulting in an inverse secondary isotope effect.[28] Further quantitative information on the activation energy for the methyl loss and the vibrational energy of 1 formed in the pertinent electronic state is needed to predict the magnitude of the secondary isotope effect and compare it with the experimental value ($k_D/k_H \sim 4$).

Conclusions

Hydrogentrimethylammonium, 1, represents a fully protonated hypervalent ammonium radical that shows metastability after being formed by vertical reduction in the gas phase. Dissociations of 1 proceed by N–H and N–C bond cleavages and show an unusual inverse isotope effect. Ab initio calculations find a very shallow potential energy minimum for the $^2A_1$ ground electronic state of 1, which is predicted to dissociate completely by loss of hydrogen. The metastability of 1 and the dissociation by loss of

(25) We thank a reviewer for suggesting these larger scale calculations.
(26) (a) Mulliken, R. S. *Acc. Chem. Res.* **1976**, *9*, 7–12. (b) Sandorfy, C. *Int. J. Quantum Chem.* **1981**, *19*, 1147–1156.

(27) (a) McDiarmid, R. *Theor. Chim. Acta* **1971**, *20*, 282. (b) Lengsfield, B. H., III; Siegbahn, P. E. M.; Liu, B. *J. Chem. Phys.* **1984**, *81*, 710–716.
(28) (a) Halevi, E. A. *Prog. Phys. Org. Chem.* **1963**, *1*, 109–221. (b) *Isotope Effects in Gas-Phase Chemistry*; Kaye, J. A., Ed.; American Chemical Society; Washington, DC, 1992.

methyl are explained by the existence of bound excited electronic states which are populated upon vertical electron transfer.[29]

Supplementary Material Available: Tables of optimized geometries and harmonic vibrational frequencies (5 pages). This material is contained in many libraries on microfiche, immediately follows this article in the microfilm version of the journal, and can be ordered from the ACS; see any current masthead page for ordering information.

(29) MP2/6-31+G(d) calculations of the doublet ground electronic state of the hydrogendimethyloxonium radical, $(CH_3)_2O^\bullet H$, predict exothermic barrierless dissociation by O–H bond cleavage. Formation of excited (Rydberg) states has been suggested to explain the existence of metastable $(CH_3)_2O^\bullet D$ (ref 8c).